Lithuanian Journal of Physics
Vol. **64**, No. 4, pp. 253–258 (2024)
ISSN 1648-8504 eISSN 2424-3647
DOI: https://doi.org/10.3952/physics.2024.64.4.6

DEPENDENCE OF TERAHERTZ PHOTOCONDUCTIVE SWITCH PERFORMANCE ON METAL CONTACT GEOMETRY

I. Nevinskas [a], M. Kamarauskas [a], A. Geižutis [a], V. Kovalevskij [a], M. Gaspariūnas [a], A. Bičiūnas [a], A. Urbanowicz [a], R. Norkus [a], and K. Ikamas [a, b, c]

[a] *Center for Physical Sciences and Technology, Saulėtekio 3, 10257 Vilnius, Lithuania*
[b] *Institute of Applied Electrodynamics and Telecommunications, Vilnius University, Saulėtekio 3, 10257 Vilnius, Lithuania*
[c] *The General Jonas Žemaitis Military Academy of Lithuania, Šilo 5A, 10322 Vilnius, Lithuania*
Email: ignas.nevinskas@ftmc.lt

Received 18 June 2024; revised 15 October 2024; accepted 15 October 2024

This study investigates the emission and spectral characteristics of photoconductive THz switches employing coplanar stripline contact geometries fabricated on a GaAs substrate. The experimental results reveal how the power outputs as well as the spectral shape are significantly influenced by the strip width dimension. Utilizing the Drude–Lorentz conductivity model, photocarrier dynamics were analyzed through an *RLC* circuit framework, offering insights into how the contact design influences the spectral response. Our findings suggest that matching the photocurrent impedance to that of the metallic contacts is critical to improving the efficiency of these devices.

Keywords: photoconductive switch, terahertz, THz, GaAs, gallium arsenide

1. Introduction

Electromagnetic waves ranging from 0.1 to 10 THz are referred to as terahertz (THz) radiation. This frequency range represents a unique gap in the electromagnetic spectrum, requiring a combination of electrical and optical methods to generate and detect the waves at room temperature. One of the most widely used devices for this purpose are the photoconductive switches. They are composed of two metal contacts placed on a short carrier lifetime semiconductor, which is photoexcited by subpicosecond laser pulses.

Terahertz emission from a photoconductive switch following picosecond laser excitation was first demonstrated by Auston in 1984 [1]. Since the introduction of this device, considerable efforts have been devoted to enhancing its optical-to-THz conversion efficiency, primarily by investigating the geometry of metal contacts [2–6], including complex designs such as log-spiral geometries [7], among others [8, 9]. However, this efficiency rarely exceeds 0.1%, except in cases where contacts are fabricated at the nanometre scale, allowing for the generation of high carrier densities through plasmonic effects [10–14] (and other works by Jarrahi and colleagues).

Despite only minor improvements in THz emission efficiency, researchers continue to search for an optimal contact geometry, as it significantly influences the spectral shape. In this study, coplanar stripline geometries fabricated on a GaAs substrate were characterized based on their emitted spectrum and average power output. Using the Drude–Lorentz conductivity model, the photocarrier dynamics were interpreted as an *RLC* circuit model, aiding in the discussion of the experimental results and providing insights for future contact design improvements.

2. Fabrication and experimental details

The switches were fabricated as follows: a layer of spin-coated photoresist was applied to the surface of a semi-insulating GaAs wafer and patterned using laser lithography (*Heidelberg Instruments*, DWL 66+) to define the contact geometries. A 10 nm titanium layer for improved adhesion,

followed by a 180 nm gold layer, was deposited via electron beam evaporation. The lift-off process was then performed in acetone. Subsequently, the wafer containing the antennas was implanted with high-energy ions to reduce the photoconductivity decay time to subpicosecond levels [16], ensuring full carrier trapping before the arrival of the next optical pulse and improving high-frequency cut-off characteristics [17]. Finally, the ultrafast photoconductive switches were separated into individual chips and mounted one by one on a hyperhemispherical high-resistivity silicon lens using a *TeraVil Ltd* mount for characterization [18].

Interestingly, as shown in Fig. 1(b), the maximum of the THz spectrum did not shift to higher frequencies despite the shorter dipole lengths. Nonetheless, spectra with a bandwidth of around 5 THz and a signal-to-noise ratio (SNR) of approximately 80 dB were recorded for all gap widths, except for some attenuation at frequencies above 1 THz in the narrower gaps, likely due to the previously mentioned shadowing.

Two experiments were conducted to assess the performance of each switch. First, the emitted THz power was measured using a broadband *Gentec EO* pyroelectric detector. The switches were positioned as close as possible to the detector to ensure that all THz radiation reached the pyroelectric module. In the second experiment, the antennas were used as coherent THz detectors in a *TeraVil Ltd* spectrometer [15] equipped with a commercial GaAs THz emitter. The first experiment utilized a laser with a wavelength of 780 nm, a repetition rate of 75 MHz and a pulse duration of 50 fs, while the second used a 780 nm, 80 MHz, 80 fs laser. As far as THz waves are concerned, the differences between the lasers are negligible.

3. Results and discussion

The classical coplanar stripline geometry shown in Fig. 1(a) has four adjustable parameters: the length, width and height of the strip, and the gap between the strips. Several studies have demonstrated that THz switch performance is influenced by both the photosensitive gap and strip width [3, 19, 20]. We examined these dependences as well, and the results are displayed in Figs. 1 and 2.

By varying the photosensitive gap width, the 50 μm gap antenna produced the most intense THz pulses (Fig. 1(a)). The gap was illuminated with a focused optical beam, obtained with a 5 cm focal length lens, resulting in a wide beam waist. The waist, measured using the sharp knife-edge method, was estimated to be 50 μm FWHM (full width at half maximum). As a result, the optical beam spot was wider than the 26 and 12 μm gaps, and parts of the spot were shadowed by the metal contacts, leading to lower emitted THz power.

The comparison of photoconductive switch performance at different strip widths is presented in Fig. 2. The most intense pulses were emitted from the 150 μm strip width geometry, while the intensity decreased at 300 μm. This suggests that within

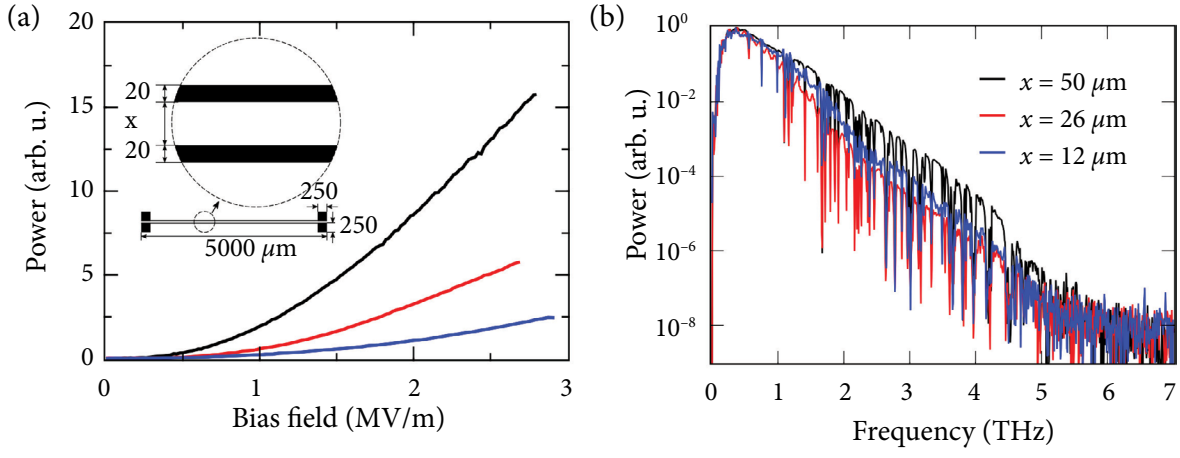

Fig. 1. A photoconductive switch with a coplanar stripline contact geometry (insert) operates at varying gap widths labelled as **x**. (a) shows the emitted THz power at different bias fields, while (b) presents the detected spectra using a *TeraVil* THz time-domain spectroscopy setup [15]. In both cases, the switches are photoexcited at 20 μJ/cm^2 fluence.

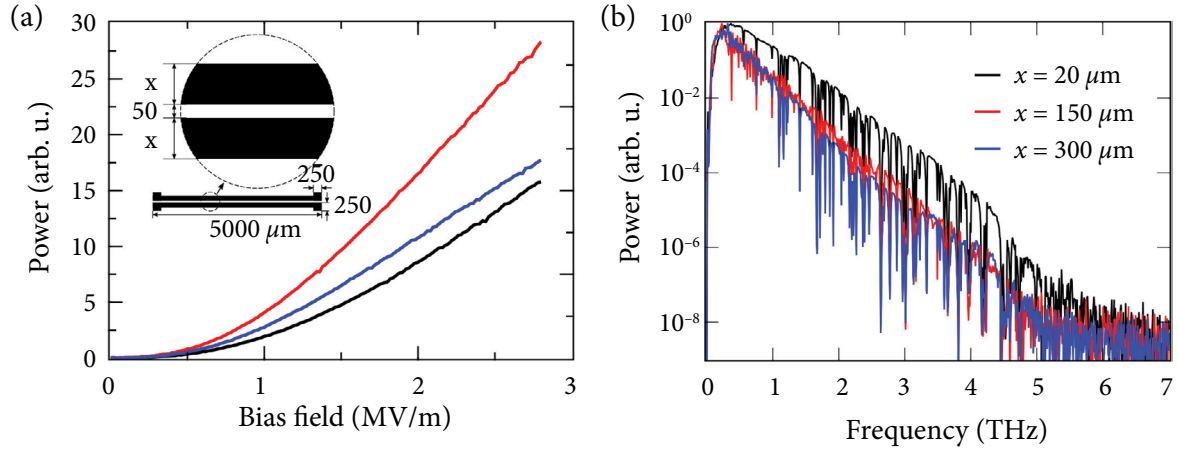

Fig. 2. Analogous to Fig. 1, except that the varied parameter is the strip width.

the 20 to 300 μm range, there is an optimal width for the maximum emission intensity, occurring when the centre wavelength of the spectrum generated by the photocarriers resonates with the metallic dipole length. The emitted average power nearly doubled, increasing from 15 to about 27 μW at the highest bias voltages.

The spectra recorded for these contact geometries clearly show a shift to lower frequencies as the strip width increases. Considering the refractive index of GaAs (n = 3.3), the half-wave resonance frequencies for strip widths of 20, 150 and 300 μm are 1.14 THz, 150 and 75 GHz, respectively. However, these estimated values do not align with the experimental results. This is expected, as the measured response is influenced by multiple factors, including the omitted gap dimension, the ultrafast photocurrent induced by the laser within the switches [21], and the nonflat spectrum illuminated onto the THz detectors. Tani et al. also demonstrated experimentally that the resonance shifted to lower frequencies with increasing the strip width. Their calculations, which take into account more geometric parameters, still did not fully match the experimental results [3, 5]. They further attributed this discrepancy to resonance peak broadening and damping.

Now, let us examine the dynamics of photoexcited carriers using the classical Drude–Lorentz conductivity model. By separating the real and imaginary parts we get

$$\sigma = \frac{ne^2\tau_s}{m^*\left(1+\mathrm{i}\omega\tau_s\right)} = \\ = \frac{ne^2\tau_s}{m^*\left(1+\omega^2\tau_s^2\right)} - \mathrm{i}\frac{ne^2\omega\tau_s^2}{m^*\left(1+\omega^2\tau_s^2\right)}, \qquad (1)$$

where n is the free carrier concentration, e is the elementary electron charge, τ_s is the mean scattering time, m^* is the effective carrier mass, and ω is the angular frequency at which the system is operating. By introducing the spatial dimensions A and l, which represent the effective volume, the photocarrier impedance Z can be expressed as follows:

$$Z = \frac{1}{\sigma}\frac{l}{A} = \frac{m^* l}{ne^2\tau_s A} + \mathrm{i}\omega\frac{m^* l}{ne^2 A}. \qquad (2)$$

A is the cross-sectional area of the photocurrent flowing between the contacts, while l is the distance travelled by the photocarriers. The photocarrier dynamics can thus be modelled as an *RLC* circuit, where Re{Z} corresponds to the resistance, representing energy losses as heat, and Im{Z} represents the reactance from carrier inertia, also known as kinetic inductance L_k [22]. Additionally, the capacitive component C arises between the spatially separated electrons and holes. This electronic circuit model works surprisingly well even at optical frequencies, particularly for modelling surface plasmons in metals [23] and optical antennas [24].

The origin of these phenomenological *RLC* components lies in the laser-induced photocurrent driven by an external voltage source, forming a series *RLC* circuit that behaves as a harmonic oscillator, governed by the second-order differential equation

$$\frac{\mathrm{d}^2 i}{\mathrm{d}t^2} + \frac{R}{L_k}\frac{\mathrm{d}i}{\mathrm{d}t} + \frac{1}{L_k C}i = 0, \qquad (3)$$

and by substituting the R, L_k, C parameters we get

$$\frac{\mathrm{d}^2 i}{\mathrm{d}t^2}+\frac{1}{\tau_\mathrm{s}}\frac{\mathrm{d}i}{\mathrm{d}t}+\omega_\mathrm{p}^2 i=0, \quad (4)$$

where ω_p is the plasma frequency. Note that this equation takes the same form as the one derived by Jepsen et al. for carrier velocity [25]. Several insights into photocarrier dynamics in THz switches can now be drawn from a classical *RLC* resonator perspective, considering a GaAs absorption depth of 1 μm, an electron overshoot velocity of $3 \cdot 10^7$ cm/s [26], a momentum scattering time of 1 ps [27] and a carrier concentration of 10^{16} cm^{-3} at ω_p = 1 THz. The ranges for the *RLC* components, the quality factor *Q* and the damping coefficient ζ for the spot diameters from 50 to 10 μm are estimated and summarized in Table 1.

When designing the most optimal contact configuration for an efficient interaction with the spectrum generated by photocarriers, two criteria must be met. First, as observed experimentally, the strip width should be approximately half the wavelength of the photocarrier spectrum. Under the typical femtosecond laser excitation, the carrier concentration ranges from 10^{15} to 10^{18} cm^{-3}, corresponding to plasma frequencies of 0.34 to 10 THz and strip widths between 3 and 67 μm. This explains the reduced emitted power from the 300 μm strip width switch. Second, the ultrafast photocurrent impedance must be matched to that of the metallic contacts.

As seen from Table 1, the resistive component of photoexcited carriers is in the order of ohms. Since the width of strips is fixed, the contact resistance can be increased by selecting the 20 times less conductive titanium rather than gold, which would appropriately increase the resistive component matching and would lower the *Q* factor. In addition, the photosensitive gap d_gap is much wider than the ballistically travelled photocarrier distance *l*. Even when considering the overshoot velocities 26], *l* is mere hundreds of nanometres. The poor photocurrent coupling into the metallic strips degrades the antenna performance by a factor of $(l/d_\mathrm{gap})^2$ [24]. To resolve this, the optical spot should be squeezed and the photosensitive gap accordingly narrowed, which would effectively shorten the transmission line between the photocarriers acting as a source and an antenna-like metal structure.

4. Conclusions

In conclusion, THz photoconductive switches with coplanar stripline contact configurations on GaAs were characterized by their emitted power

Table 1. Photoexcited carrier dynamics in THz switches modelled as an *RLC* circuit. The *RLC* values are estimated at 1 THz for spot diameters ranging from 50 to 10 μm.

	Electronics	Optoelectronics	Value at 1 THz
Resistance, Re{*Z*}	R	$\frac{m^* l}{ne^2\tau_\mathrm{s}A}$	1–7 Ω
Inductance, Im{*Z*}	L	$L_\mathrm{k}=\frac{m^* l}{ne^2 A}$	1–7 pH
Capacitance	C	$\frac{\varepsilon_\mathrm{r}\varepsilon_0 A}{l}$	3–16 fF
Resonance	$\omega=\frac{1}{\sqrt{LC}}$	$\omega_\mathrm{p}=\sqrt{\frac{ne^2}{m^*\varepsilon_\mathrm{r}\varepsilon_0}}$	$n = 10^{16}$ cm^{-3}
Quality factor, *Q*	$\frac{1}{R}\sqrt{\frac{L}{C}}$	$\omega_\mathrm{p}\tau_\mathrm{s}$	6
Damping coef., ζ	$\frac{R}{2}\sqrt{\frac{C}{L}}$	$\frac{1}{2\omega_\mathrm{p}\tau_\mathrm{s}}$	0.08

and detected spectra across varying strip and gap widths. The experimental results confirmed the validity of the half-wave dipole rationale, though the accurate resonance frequency estimation requires accounting for photoexcitation conditions and metal properties. By applying the Drude–Lorentz conductivity model and *RLC* circuit analysis, it was demonstrated that the spectrum generated by photocarriers demanded a low *Q* factor antenna design, balancing the trade-off between the metal conductivity and the spectral bandwidth. Lastly, the results highlight the need for further investigation into the photosensitive gap dimension, which is crucial to the effective photocurrent coupling to the metallic structure.

Acknowledgements

The work has been funded by the Research Council of Lithuania, Grant Lietuvos Mokslo Taryba, S-TPP-23-11.

References

[1] D.H. Auston, K.P. Cheung, and P.R. Smith, Picosecond photoconducting Hertzian dipoles, Appl. Phys. Lett. **45**, 284 (1984).

[2] Y. Cai, I. Brener, J. Lopata, J. Wynn, L. Pfeiffer, and J. Federici, Design and performance of singular electric field terahertz photoconducting antennas, Appl. Phys. Lett. **71**, 2076 (1997).

[3] M. Tani, S. Matsuura, K. Sakai, and S.-I. Nakashima, Emission characteristics of photoconductive antennas based on low-temperature-grown GaAs and semi-insulating GaAs, Appl. Opt. **36**, 7853 (1997).

[4] P.J. Hale, J. Madeo, C. Chin, S.S. Dhillon, J. Mangeney, J. Tignon, and K.M. Dani, 20 THz broadband generation using semi-insulating GaAs interdigitated photoconductive antennas, Opt. Express **22**, 26358 (2014).

[5] F. Miyamaru, Y. Saito, K. Yamamoto, T. Furuya, S. Nishizawa, and M. Tani, Dependence of emission of terahertz radiation on geometrical parameters of dipole photoconductive antennas, Appl. Phys. Lett. **96**, 211104 (2010).

[6] S. Alfihed, I.G. Foulds, and J.F. Holzman, Characteristics of bow-tie antenna structures for semi-insulating GaAs and InP photoconductive terahertz emitters, Sensors **21**, 3131 (2021).

[7] X. Zhang, F. Zhan, X. Wei, W. He, and C. Ruan, Performance enhancement of photoconductive antenna using saw-toothed plasmonic contact electrodes, Electronics **10**, 2693 (2021).

[8] D.R. Bacon, J. Madéo, and K.M. Dani, Photoconductive emitters for pulsed terahertz generation, J. Opt. **23**, 064001 (2021).

[9] K. Anusha, D. Mohana Geetha, and A. Amsaveni, *Advances in Terahertz Technology and its Applications*, eds. S. Das, N. Anveshkumar, J. Dutta, A. Biswas (Springer, 2021) pp. 337–362.

[10] B. Heshmat, H. Pahlevaninezhad, Y. Pang, M. Masnadi-Shirazi, R. Burton Lewis, T. Tiedje, R. Gordon, and T.E. Darcie, Nanoplasmonic terahertz photoconductive switch on GaAs, Nano Lett. **12**, 6255 (2012).

[11] A. Jooshesh, L. Smith, M. Masnadi-Shirazi, V. Bahrami-Yekta, T. Tiedje, T.E. Darcie, and R. Gordon, Nanoplasmonics enhanced terahertz sources, Opt. Express **22**, 27992 (2014).

[12] S.-H. Yang, M.R. Hashemi, C.W. Berry, and M. Jarrahi, 7.5% optical-to-terahertz conversion efficiency offered by photoconductive emitters with three-dimensional plasmonic contact electrodes, IEEE Trans. Terahertz Sci. Technol. **4**, 575 (2014).

[13] S. Lepeshov, A. Gorodetsky, A. Krasnok, N. Toropov, T.A. Vartanyan, P. Belov, A. Alú, and E.U. Rafailov, Boosting terahertz photoconductive antenna performance with optimised plasmonic nanostructures, Sci. Rep. **8**, 6624 (2018).

[14] M. Bashirpour, J. Poursafar, M. Kolahdouz, M. Hajari, M. Forouzmehr, M. Neshat, H. Hajihoseini, M. Fathipour, Z. Kolahdouz, and G. Zhang, Terahertz radiation enhancement in dipole photoconductive antenna on LT-GaAs using a gold plasmonic nanodisk array, Opt. Laser Technol. **120**, 105726 (2019).

[15] TeraVil Ltd | T-SPEC Real-Time Terahertz Spectrometer.

[16] A. Krotkus, K. Bertulis, R. Adomavičius, V. Pačebutas, and A. Geižutis, Semiconductor materials for ultrafast optoelectronic applications, Lith. J. Phys. **49**, 359 (2009).

[17] L. Duvillaret, F. Garet, J.-F. Roux, and J.-L. Coutaz, Analytical modeling and optimization of terahertz time-domain spectroscopy experiments, using photoswitches as antennas, IEEE J. Sel. Top. Quantum Electron. **7**, 615 (2001).

[18] TeraVil Ltd | THz Emitter/Detector Mounting Stage.

[19] Y. Cai, I. Brener, J. Lopata, J. Wynn, L. Pfeiffer, and J. Federici, Design and performance of singular electric field terahertz photoconducting antennas, Appl. Phys. Lett. **71**, 2076 (1997).

[20] F. Miyamaru, Y. Saito, K. Yamamoto, T. Furuya, S. Nishizawa, and M. Tani, Dependence of emission of terahertz radiation on geometrical parameters of dipole photoconductive antennas, Appl. Phys. Lett. **96**, 211104 (2010).

[21] P. Smith, D. Auston, and M. Nuss, Subpicosecond photoconducting dipole antennas, IEEE J. Quantum Electron. **24**, 255 (1988).

[22] D.A. Cardwell and D.S. Ginley, *Handbook of Superconducting Materials*, 1st ed. (CRC Press, 2002).

[23] M. Staffaroni, J. Conway, S. Vedantam, J. Tang, and E. Yablonovitch, Circuit analysis in metal-optics, Photonics Nanostructures: Fundam. Appl. **10**, 166 (2012).

[24] M.S. Eggleston, K. Messer, L. Zhang, E. Yablonovitch, and M.C. Wu, Optical antenna enhanced spontaneous emission, PNAS **112**, 1704 (2015).

[25] P.U. Jepsen, R.H. Jacobsen, and S.R. Keiding, Generation and detection of terahertz pulses from biased semiconductor antennas, J. Opt. Soc. Am. B **13**, 2424 (1996).

[26] A. Reklaitis, A. Krotkus, and G. Grigaliunaite, Enhanced drift velocity of photoelectrons in a semiconductor with ultrafast carrier recombination, Semicond. Sci. Technol. **14**, 945 (1999).

[27] M. Bernardi, D. Vigil-Fowler, C.S. Ong, J.B. Neaton, and S.G. Louie, Ab initio study of hot electrons in GaAs, PNAS **112**, 5291 (2015).

TERAHERCINIŲ FOTOJUNGIKLIŲ CHARAKTERISTIKŲ PRIKLAUSOMYBĖS NUO METALINIŲ KONTAKTŲ GEOMETRIJOS

I. Nevinskas [a], M. Kamarauskas [a], A. Geižutis [a], V. Kovalevskij [a], M. Gaspariūnas [a], A. Bičiūnas [a], A. Urbanowicz [a], R. Norkus [a], K. Ikamas [a, b, c]

[a] *Fizinių ir technologijos mokslų centras, Vilnius, Lietuva*

[b] *Vilniaus universiteto Taikomosios elektrodinamikos ir telekomunikacijų institutas, Vilnius, Lietuva*

[c] *Generolo Jono Žemaičio Lietuvos karo akademija, Vilnius, Lietuva*

Santrauka

Tiriamos terahercinių fotojungiklių ant GaAs padėklo emisijos ir spektro charakteristikų priklausomybės nuo koplanarinių juostelių kontaktų geometrijos. Eksperimentiškai parodoma, kaip stipriai keičiasi išspinduliuojama galia bei spektro forma nuo kontaktinės juostelės pločio. Naudojantis Drude ir Lorentz elektrinio laidumo modeliu, fotokrūvininkų dinamika išanalizuota *RLC* grandinės modelyje, suteikiančiame įžvalgų apie kontaktų dizaino įtaką fotojungiklių atsakui. Nustatėme, kad suderinti fotosrovės impedansą su metalinių kontaktų impedansu yra kertinis reikalavimas šių prietaisų našumui padidinti.